Rain-affected radiance data performance in 4D-Var

Carla Cardinali and Fernando Prates

ECMWF, Reading, UK

Abstract

In this paper, a comprehensive assessment of the impact of rain-affected radiances observations in the operational ECMWF assimilation and forecast system is presented using advanced diagnostic tools. In particular, the observation influence in the assimilation process and the related contribution on the short-range forecast error of radiance observations from microwave sensors is evaluated with recently developed diagnostic tools based on the adjoint version of the model. The recent operational changes on the assimilation of these observations result in a more beneficial impact on the initial condition and the short-range forecast. The largest information content is obtained for observations that are located in clear sky regions as indicated by the model short-range forecast and the observations themselves. However, the largest decrease of the forecast error is provided by observations detected in cloudy regions. The usage of Special Sensor Microwave /Imager data help reducing model systematic errors in the central eastern equatorial Pacific where the ITCZ is located and the Arabian sea where the Monsoon season is taking place.

1. Introduction

Over the last decade, data assimilation schemes have evolved towards very sophisticated systems, such as the four-dimensional variational system (4D-Var) (Rabier *et al.* 2000) that operates at the European Centre for Medium-Range Weather Forecasts (ECMWF). The scheme handles a large variety of both space and surface-based meteorological observations. It combines the observations with prior (or background) information on the atmospheric state and uses a comprehensive (linearized) forecast model to ensure that the observations are given a dynamically realistic, as well as statistically likely response in the analysis. Effective performance monitoring of such a complex system, with an order of 10^8 degrees of freedom and more than 10^7 observations per 12-hour assimilation cycle, has become an absolute necessity.

The assessment of each observation contribution to the analysis is among the most challenging diagnostics in data assimilation and numerical weather prediction. Methods have been derived to measure the observational influence in data assimilation schemes (Purser and Hung 1993, Cardinali *et al*. 2004, Fisher 2003, and Chapnick *et al*. 2004). These techniques show how the influence is assigned during the assimilation procedure, which partition is given to the observation and which is given to the background or pseudo-observation. They therefore provide indication of the robustness of the fit between model and observations and allow some tuning of the weights assigned in the assimilation system. Measures of the observational influence are useful for understanding the DA scheme itself: How large is the influence of the latest data on the analysis and how much influence is due to the background? How much would the analysis change if one single influential observation were removed? How much information is extracted from the available data?

To answer these questions it was necessary to consider the diagnostic methods that have been developed for monitoring statistical multiple regression analyses and 4D-Var is a special case of the Generalized Least Square (GLS) problem (Talagrand, 1997) for weighted regression, thoroughly investigated in the statistical literature.

Recently, adjoint-based observation sensitivity techniques have been used (Baker and Daley 2000, Langland and Baker 2004, Cardinali and Buizza, 2004, Morneau *et al*., 2006, Zhu and Gelaro 2008, Cardinali 2009) to measure the observation contribution to the forecast, where the observation impact is evaluated with respect to a scalar function representing the short-range forecast error. In general, the adjoint methodology can be used to estimate the sensitivity measure with respect to any parameter of importance of the assimilation system. Very recently, Daescu (2008) and Daescu and Todling (2010) derived a sensitivity equation of an unconstrained variational data assimilation system from the first order necessary condition with respect to the main input parameters: observation, background and their error covariance matrices. The paper provides the theoretical framework for further diagnostic tool development not only to evaluate the observation impact on the forecast but also the impact of the other analysis parameters. Sensitivity to background covariance matrix can help in evaluating the correct specification of the background weight and their correlation. Limitations and weaknesses of the covariance matrices are well known, several assumptions and simplifications are made to derive them. Desroziers and Ivanov (2001) and Chapnik et al. (2006) discussed the importance of diagnosing and tuning the error variances in a data assimilation scheme.

The adjoint-based observation sensitivity technique measures the impact of observations when the entire observation dataset is present in the assimilation system. It also measures the response of a single forecast metric to all perturbations of the observing system. It provides the impact of all observations assimilated at a single analysis time.

The adjoint-based technique is limited by the tangent linear assumption, valid up to 3 days. Furthermore, a simplified adjoint model is usually used to carry the forecast error information backwards, which limits further the validity of the linear assumption, and therefore restricts the use of the diagnostic to a typical forecast range of 24-48 hours.

In this paper, a comprehensive assessment of the impact of all-sky microwave imager radiances in the assimilation and forecast system is provided throughout the diagnostic tools introduced above. All-sky assimilation of microwave imager radiances became operational in March 2009 (Bauer et al., 2010; Geer et al., 2010). In the all-sky approach, radiance observations from Special Sensor Microwave /Imager (SSM/I, Hollinger et al., 1990) and Advanced Microwave Scanning Radiometer for the Earth Observing System (AMSR-E, Kawanishi *et al*., 2003) are assimilated in all conditions, whether clear, cloudy or rainy. At the frequencies used by microwave imagers, the atmosphere is semi-transparent except in heavy cloud and precipitation conditions. Observations are only assimilated over oceans where the observations are sensitive to ocean surface properties (e.g. surface temperature and wind-speed), atmospheric water vapour, cloud and precipitation.

Recently, a complete revision of observation error variance, quality control, thinning and resolution-matching of the all-sky assimilation of microwave imagers was implemented in the operational ECMWF 4D-Var system.

Observation error variance definition and bias correction make use of information from both model forecast and observations. Because cloud and precipitation structures are often misplaced in the model forecast a variational bias correction that is only based on model information would often misrepresent cases where model and observations disagree on the sky representation. The model is also used to provide observation error variances that increase with the mean amount of clouds indicated by the model and the observations (Geer and Bauer 2010). The spatial scale of the observations has also been examined. Instead of taking the nearest single all-sky observation to a grid point, an average or 'superob' of all observations falling into a grid box is calculated prior to the assimilation. Also, the new approach screens out observations where the model shows 'cold sector' and 'heavy snowfall' biases. These biases are in fact too difficult to deal using a predictor-based bias correction scheme.

The paper is organized as follows: section 2 and 3 describe the mathematical framework of the adjoint tools used in the investigation. Section 4 presents the results and conclusions are shown in section 5.

2. Analysis and Forecast Observational influence for DA scheme

2.1. Linear statistical estimation in Numerical Weather Prediction

Data assimilation systems for NWP provide estimates of the atmospheric state $\mathbf{x}$ by combining meteorological observations $\mathbf{y}$ with prior (or background) information $\mathbf{x}_b$. A simple Bayesian Normal model provides the solution as the posterior expectation for $\mathbf{x}$, given $\mathbf{y}$ and $\mathbf{x}_b$. The same solution can be achieved from a classical *frequentist* approach, based on a statistical linear analysis scheme providing the Best Linear Unbiased Estimate (Talagrand, 1997) of $\mathbf{x}$, given $\mathbf{y}$ and $\mathbf{x}_b$. The optimal GLS solution to the analysis problem (see Lorenc, 1986) can be written

$$\mathbf{x}_a = \mathbf{K}\mathbf{y} + (\mathbf{I}_n - \mathbf{K}\mathbf{H})\mathbf{x}_b \qquad 2.1$$

The vector $\mathbf{x}_a$ is the 'analysis'. The gain matrix $\mathbf{K}$ ($n \times p$) takes into account the respective accuracies of the background vector $\mathbf{x}_b$ and the observation vector $\mathbf{y}$ as defined by the $n \times n$ covariance matrix $\mathbf{B}$ and the $p \times p$ covariance matrix $\mathbf{R}$, with

$$\mathbf{K} = (\mathbf{B}^{-1} + \mathbf{H}^T\mathbf{R}^{-1}\mathbf{H})^{-1}\mathbf{H}^T\mathbf{R}^{-1} \qquad 2.2$$

Here, $\mathbf{H}$ is a $p \times n$ matrix interpolating the background fields to the observation locations, and transforming the model variables to observed quantities (e.g. radiative transfer calculations transforming the models temperature, humidity and ozone into brightness temperatures as observed by several satellite instruments). In the 4D-Var context introduced below, $\mathbf{H}$ is defined to include also the propagation in time of the atmospheric state vector to the observation times using a forecast model.

Substituting (3.2) into (3.1) and projecting the analysis estimate onto the observation space, the estimate becomes

$$\hat{\mathbf{y}} = \mathbf{H}\mathbf{x}_a = \mathbf{H}\mathbf{K}\mathbf{y} + (\mathbf{I}_p - \mathbf{H}\mathbf{K})\mathbf{H}\mathbf{x}_b \qquad 2.3$$

It can be seen that the analysis state in observation space ($\mathbf{Hx_a}$) is defined as a sum of the background (in observation space, $\mathbf{Hx_b}$) and the observations $\mathbf{y}$, weighted by the $p \times p$ square matrices $\mathbf{I-HK}$ and $\mathbf{HK}$, respectively.

In this case, for each unknown component of $\mathbf{Hx}$, there are two data values: a real and a 'pseudo' observation. The additional term in (2.3) includes these pseudo-observations, representing prior knowledge provided by the observation-space background $\mathbf{Hx_b}$. The analysis sensitivity with respect to the observations is obtained (Cardinali et al 2004):

$$\mathbf{S} = \frac{\partial \hat{\mathbf{y}}}{\partial \mathbf{y}} = \mathbf{K}^T \mathbf{H}^T \qquad 2.4$$

We focus here on the (2.4) expression..The (projected) background influence is complementary to the observation influence. For example, if the self-sensitivity with respect to the ith observation is S_{ii}, the sensitivity with respect the background projected at the same variable, location and time will be simply 1-S_{ii}.

In particular, the observation influence S_{ii}=[0,1] where S_{ii}=0 means that the ith observation has had no influence at all in the analysis (only the background counted) and S_{ii}=1 indicates that an entire degree of freedom has been devoted to fit that data point (the background has had no influence). The tr(**S**) can be interpreted as a measure of the amount of information extracted from the observation or 'degree of freedom for signal' (DFS) whilst it follows that the complementary trace, tr(**I**–**S**)=p–tr(**S**), is the *DF* for background. That is the weight given to prior information, to be compared to the observational weight tr(**S**).

3. Forecast sensitivity to the observations

Baker and Daley (2000) derived the forecast sensitivity equation with respect to the observations in the context of variational data assimilation. Let us consider a scalar J-function of the forecast error. Then, the sensitivity of J with respect to the observations can be written using a simple derivative chain as:

$$\frac{\partial J}{\partial \mathbf{y}} = \frac{\partial J}{\partial \mathbf{x}_a} \frac{\partial \mathbf{x}_a}{\partial \mathbf{y}} \qquad 3.1$$

$\partial J / \partial \mathbf{x}_a$ is the sensitivity of forecast error to initial condition $\mathbf{x}_a$ (Rabier et al. 1996, Gelaro et al., 1998) where the forecast error is expressed as dry energy norm . From (2.1) the sensitivity of the analysis system with respect to the observations and the background can be derived from:

$$\frac{\partial \mathbf{x}_a}{\partial \mathbf{y}} = \mathbf{K}^T \qquad 3.2$$

By using (3.2) and (2.2) the forecast sensitivity to the observations becomes:

$$\frac{\partial J}{\partial \mathbf{y}} = \mathbf{K}^T \frac{\partial J}{\partial \mathbf{x}_a} = \mathbf{R}^{-1}\mathbf{H}(\mathbf{B}^{-1} + \mathbf{H}^T\mathbf{R}^{-1}\mathbf{H})^{-1} \frac{\partial J}{\partial \mathbf{x}_a} \qquad 3.3$$

A second order sensitivity gradient needs to be considered in 3.3 (Langland and Baker 2004; Errico 2007) because only superior orders than first contain the information related to the forecast error. In fact, the first order one only contains information on the sub-optimality of the assimilation system (Cardinali 2009).

The variation δJ of the forecast error expressed by J can be found by rearranging (3.1) and by using the adjoint property for the linear operator:

$$\delta J = \left\langle \frac{\partial J}{\partial \mathbf{x}_a}, \delta \mathbf{x}_a \right\rangle = \left\langle \frac{\partial J}{\partial \mathbf{x}_a}, \mathbf{K}(\mathbf{y} - \mathbf{H}\mathbf{x}_b) \right\rangle = \left\langle \mathbf{K}^T \frac{\partial J}{\partial \mathbf{x}_a}, \mathbf{y} - \mathbf{H}\mathbf{x}_b \right\rangle = \left\langle \mathbf{K}^T \frac{\partial J}{\partial \mathbf{x}_a}, \delta \mathbf{y} \right\rangle = \left\langle \frac{\partial J}{\partial \mathbf{y}}, \delta \mathbf{y} \right\rangle \quad 3.5$$

where $\delta \mathbf{x}_a = \mathbf{x}_a - \mathbf{x}_b$ are the analysis increments and $\delta \mathbf{y} = \mathbf{y} - \mathbf{H}\mathbf{x}_b$ is the innovation vector. The sensitivity gradient $\partial J / \partial \mathbf{x}_a$ is valid at the starting time of the 4D-Var window (typically 09 and 21 UTC for the 12h 4D-Var set-up used at ECMWF). As for **K**, its adjoint $\mathbf{K}^T$ incorporates the temporal dimension, and the δ**y** innovations are distributed over the 12-hour window. The variation of the forecast error due to a specific measurement can be summed up over time and space in different subsets to compute the average contribution of different component of the observing system to the forecast error. For example, the contribution of all AMSU-A satellite instruments, *s*, and channels, *i*, over time T will be:

$$\delta J_{AMSU-A} = \sum_{\substack{s \in S \\ t \in T}} \sum_{i \in channel} \delta J^{s}_{it}$$

The forecast error contribution can be gathered over different subsets that can represent a specific observation type, a specific vertical or horizontal domain, or a particular meteorological variable.

4. Results

Analysis and forecast experiments using the ECMWF 4D-Var system (Rabier *et al* 2000; Janiskova *et al*. 2002; Lopez and Moreau, 2005) have been performed for June 2009 to assess, in particular, the impact of SSM/I and AMSR-E microwave imagers observations, sensitive to humidity, cloud, precipitation and ocean surface (Geer and Bauer 2010). The 24-hour forecast error contribution (FEC) of the all observing system components is computed and shown in Figure 1. The largest contribution in decreasing the forecast error is provided by AMU-A (~16%), IASI and AIRS (12%) followed by AIREP (aircraft data 10%), TEMP (radiosonde 7%), GPS-RO (6%) and SCAT data (5%). All the other observations contribute up to 4%. The Special Sensor Microwave Imager/Sounder, SSM/I, decrease the 24-hour forecast error by 4% and the Advanced Microwave Scanning Radiometer-Earth Observing System, AMSR-E, by 2% being SSM/I the largest contribution among radiance data sensitive to humidity. Table 1 summarizes the window channels from the two microwave sensors used in this study. SSM/I is a conical scanning passive microwave imager on board on the latest generation of the DMSP satellites since June 1987. Observations are acquired at four frequencies (19.3, 22.2, 37.0 and 85.5 GHz), with a dual polarization (only horizontal at 22.2 GHz) and near constant zenith angle of 53^o. The instrument makes measurements at the mean altitude of 830 km with a swath width of 1400 km and horizontal resolution from 12.5 km (at 85.5 GHz) to 25 km (at 19.3 GHz). In addition to SSM/I, AMSR-E data have been assimilated. AMSR-E instrument is operating aboard NASA's

Aqua satellite since4 May 2002. It is a twelve-channel, six-frequency, passive-microwave radiometer system with a near constant zenith angle of about 55o. It measures horizontally and vertically polarized brightness temperatures at 6.9, 10.7, 18.7, 23.8, 36.5, and 89.0 GHz. At an altitude of 705 km, AMSRE measures the upwelling scene brightness temperatures with a swath width of 1445 km and a horizontal resolution.

The observation influence of microwave imager data can also be computed and compared with the forecast error reduction for all the channels assimilated. Figure 2 shows the DFS (tr(**S**), (a)) and FEC (b) for the five SSM/I channels used and for the different flags applied to the observations.

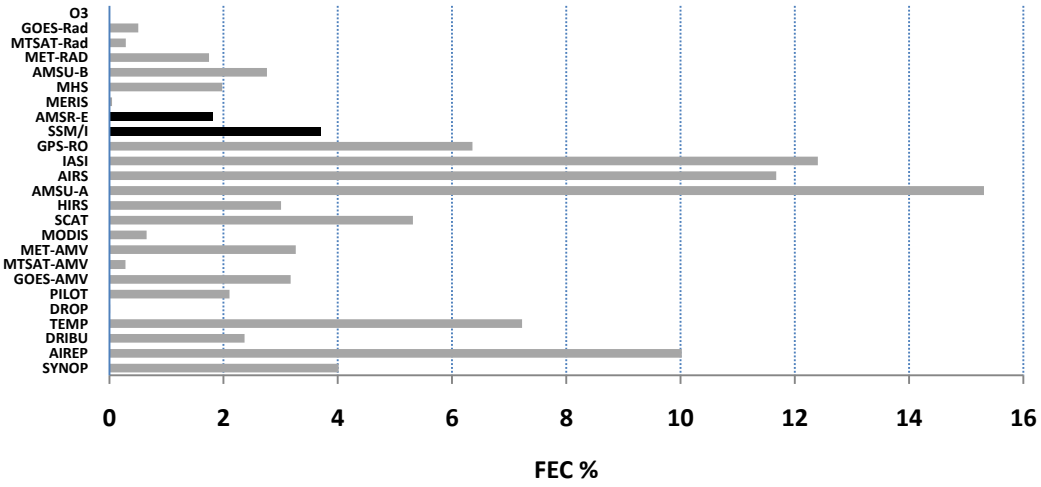

Figure 1: 24-hour forecast error contribution in percentage for June 2009 and all the observation types assimilated

	Channel	Frequency	Polarization
SSM/I	1	19.35	V
	2	19.35	H
	3	22.235	V
	4	37.0	V
	5	37.0	H
	6	85.0	V
AMSR-E	5	18.7	V
	6	18.7	H
	7	23.8	V
	8	23.8	H
	9	36.5	V

Table1: Window channels from microwave sensors

The flags are given during the assimilation process accordingly to the model background (12 hour forecast) and observation cloudiness information: flag-Clear and flag-Cloudy means that model and observation are consistently indicating that the measurement is in clear-sky or in cloudy-sky area, respectively. Flag-OBS-Clear and OBS-Cloudy indicates that observation and first guest provide different information on cloudiness: whereas the observation denotes a clear-sky measurement, the first guess at the same location registered clouds and vice-versa (Geer and Bauer 2010).

From fig 2a, the largest contribution in the analysis is provided by flag-Clear from a maximum of 18% (channel 1) to 5% (channel 6). The first two SSM/I channels have strong sensitivity to surface wind while channels 3 and 6 are dominated by water vapour. All the other flags show very similar DFS that varies from 5% (channel 1) to 1% (channel 6). Flag-Clear (both observation and background in clear sky) also presents the largest observation influence (S_{ii} or mean influence per measurement) for all channels (not shown) whilst all the other flags exhibit a different observation influence ranking with respect to the DFS. In particular, flag-Cloudy, with the second largest DFS has the least observation influence (0.15), indicating that the DFS was in this flag-case affected more by the number of observations (larger than for OBS-Clear or OBS-Cloudy flags) than by the single measurement influence. Measurements in cloudy areas are expected to be less influential since for example the observation error variance is assumed to increase proportional to the clouds amount. On the 24-hour forecast impact, the largest contribution to the decrease of forecast error is due to flag-Cloudy observations (fig 2b) and in particular from a maximum of ~12% (channel 3) to a minimum of 3% (channels 6 and 4). The smallest forecast contribution is provided by observations flagged OBS-Clear that count also the smallest DFS.

Similar impact in the analysis and the short-range forecast is noticed for AMSR-E radiances. In particular for AMSR-E, the per channel impact distribution is different, likely due to the fact that the instrument has also a horizontal polarized 24 GHz channel with strong sensitivity to water vapour which enhances the contribution of both channel 7 and 8. Figure 3 show DFS (a) and FEC (b) for all AMSR-E channels assimilated. The largest DFS is provided by flag-Clear observations (~17% channel 8) whilst the largest forecast error decrease is due to flags-Cloudy observations (~17% channel 8). The smallest DFS and FEC contribution is from observations flagged OBS-Cloudy and OBS-Clear, respectively.

In general, the assimilation of humidity sensitive radiances from microwave instruments show the largest analysis influence when observations together with the first-guess indicate that the measurement is taken in clear sky areas but the largest contribution to the 24-hour forecast error comes instead from observations taken (accordingly to the measurement and first-guess indication) in cloudy-areas. Several reasons can explain this: cloudy areas are believed to be the regions where the forecast error is faster propagating, consequently, observations can stronger contribute to reduce the error than in other regions where the forecast error is much smaller. Both DFS and FEC depend on the transpose Kalman gain matrix $\mathbf{K}^T$, FEC also depends on the forecast error and in particular FEC is modulated by the percentage of forecast error that projects on $\mathbf{K}^T$. Errors in the verification analysis (the analysis used to compute the forecast error) would under or over estimate the forecast error and its projection on $\mathbf{K}^T$ and the total effect will be manifest on a decrease or increase (respectively) of impact with respect to the DFS. In numerical weather prediction, since the 'truth' is unknown, the analysis is used, being the best representation of the truth, to compute the forecast error. In the near

future satellite data, providing a homogeneous and dense data coverage, can be also used to provide a independent forecast error estimation.

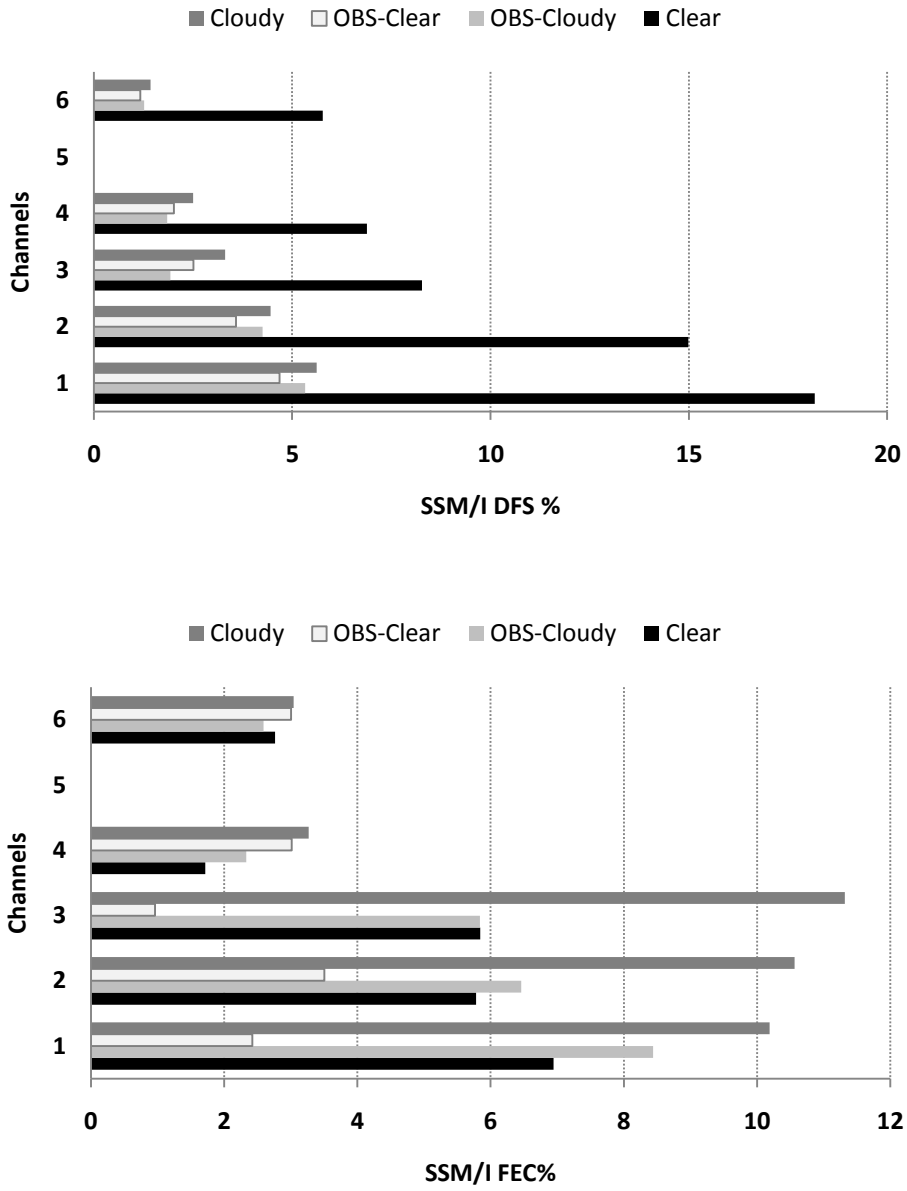

Figure 2: DFS (a) and FEC (b) in percentage per SSM/I assimilated channels

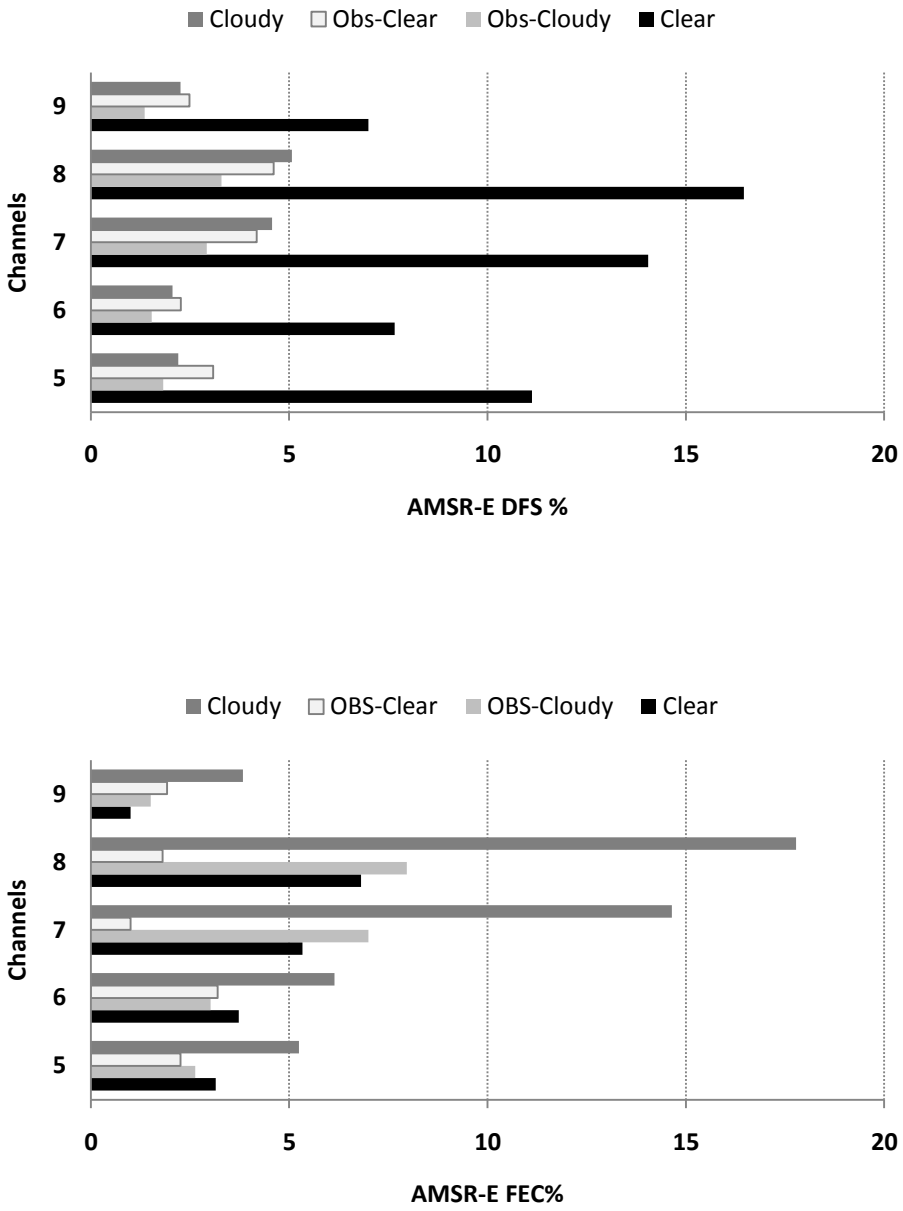

Figure 3: DFS (a) and FEC (b) in percentage per AMSR-E assimilated channels

Observation influence and forecast impact with respect to a particular data type can be geographically mapped. Figure 4a shows the average observation influence for SSM/I radiances and for all the cloudiness flags considered. The largest contribution in the analysis is observed in the tropical and sub-tropical (for the northern hemisphere) band and follows the distribution of water vapour and precipitation: over the Pacific ocean along the mean position of the ITCZ (S_{ii}=0.25), the Golf of Mexico (S_{ii}=0.38) and Indian summer Monsoon region (OI=0.35-0.4). No significant differences on observation influence patterns are observed among the different data-flags i.e. in clear skies the larger observation sensitivities follow the water vapour patterns. FEC is illustrated in fig.4b where negative (blue shading contour) and positive (red shading colour) values means decrease and increase of forecast error, respectively. A quite consistent reduction of 24 hour forecast error is observed almost

everywhere. Some forecast degradation (positive values) areas can be noticed over the western Pacific, the Indian ocean and on the Pacific ocean close to the South American continent. Interestingly, different flag-types correspond to different FEC patterns (not shown). In particular, the all-sky flags pattern (fig. 4b) is very similar to the OBS-Cloudy flag pattern for the tropical band.

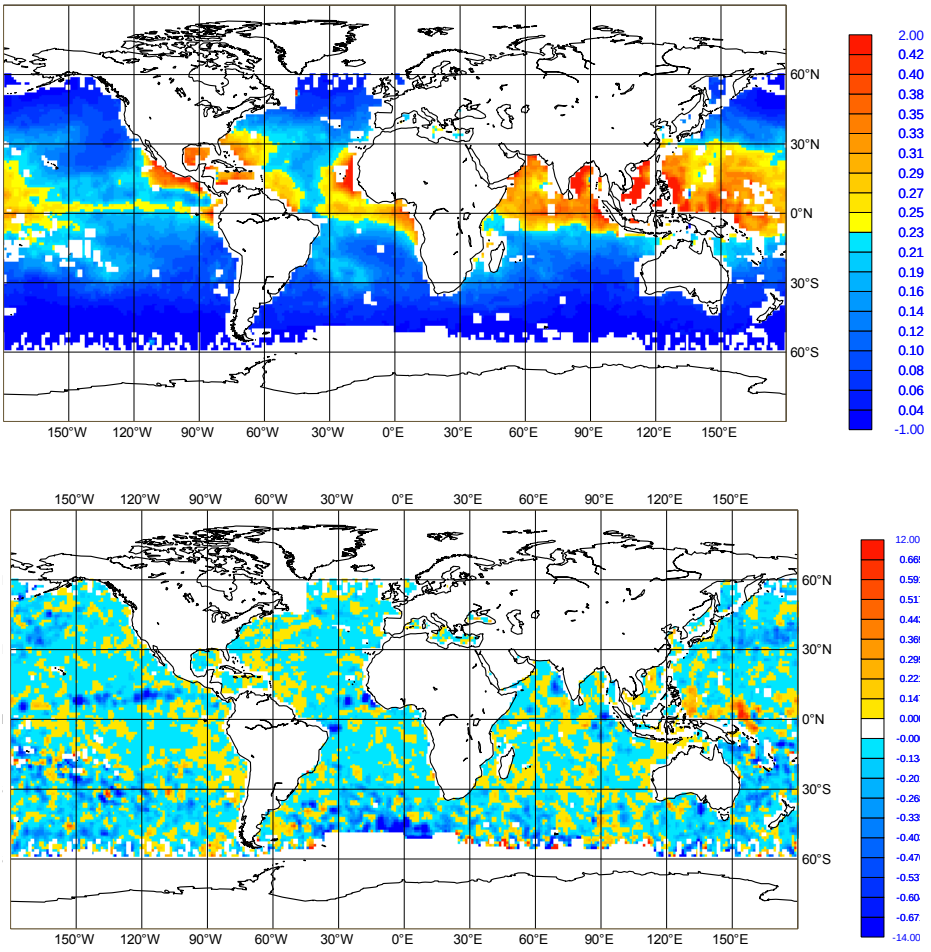

Figure 4: SSM/I All-sky radiances OI ((a), non-dimensional unit) and FEC ((b), Joule unit) averaged over June 2009

Two areas of forecast impact will be analyzed in more detail: the central eastern equatorial Pacific where the ITCZ is located, and the Arabian Sea where the Monsoon season is taking place. From fig. 4(b) SSM/I largely contribute to decrease the forecast error along the mean position of ITCZ. To assess the SSM/I impact, an Observation System Experiment (OSE) has been performed with and without the assimilation of these data. Figure 5 shows the zonal average cross section between 150° to 110° W of the mean analysis differences with and without SSMI/I for June 2009. SSM/I reduce the amount of humidity at low level (~850 hPa) by a maximum of 4% whilst near the surface the relative humidity content increases on average by 2% (fig 5a) from 0° to 20° N. The indirect impact on the

circulation can be seen on fig.5b where the vertical velocity cross section mean differences (10^{-2} Pa/s) indicate in intensification of the rising motion, associated with the mean position of the ITCZ. In particular, the main convective cell around 8° N depicts an increased upward motion of 0.04 Pa/s that results on an intensification of the circulation convergence in the lower atmosphere (not shown). The total SSM/I effect is therefore to reinforce the dominant branch of the Hadley circulation in the Northern Hemisphere, which is known to be persistently weak in the ECMWF forecast model.

In the Arabian Sea, June is dominated by the initiation of the Indian summer Monsoon circulation. From fig 4b, a general decrease of the 24 hour forecast error is noticed with larger impact close to the Arabic peninsula and the India continent. The OSE in that area shows an average reduction of the relative humidity up to 6% in the troposphere, below 500 hPa, between the equator and 18 N (fig 6a) when SSM/I microwave radiances are assimilated.

The indirect effect on the wind field can be summarized from fig.6b (meridional wind not shown). The mean differences indicate stronger near surface southwesterly wind when SSM/I is included. In the low troposphere (~850hPa) the analysed winds tend to increase close to the equator whilst the westerly component of the wind is reduced in the region above 12°N.

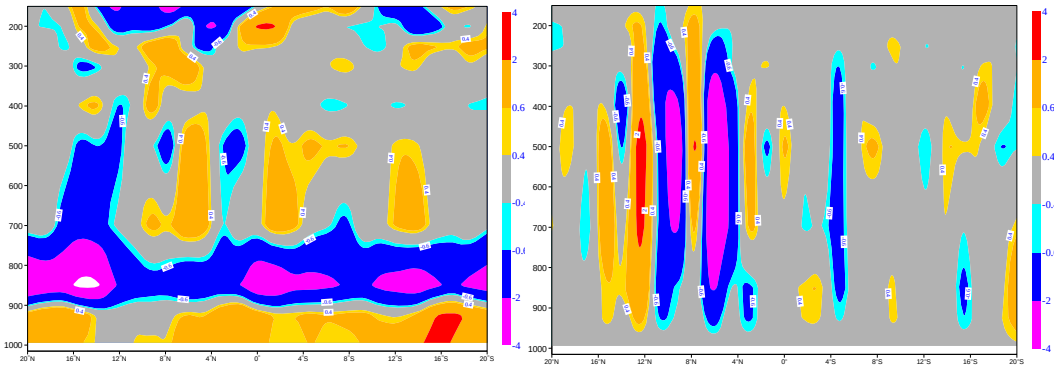

Figure 5: Zonal average cross section (150-110° W) of the mean analysis differences between with and without the assimilation of SSM/I for June 2009. (a) relative humidity (%); (b) vertical velocity (10^{-2} Pa/s)

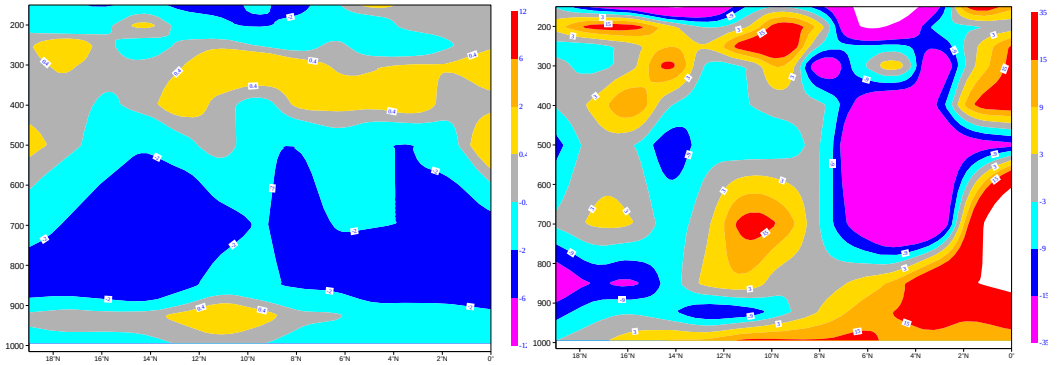

Figure 6: Zonal average cross section (50-71° E) of the mean analysis differences between with and without the assimilation of SSM/I for June 2009. (a) relative humidity (%); (b) zonal wind (10^{-2} ms^{-1})

5. Conclusions

Over the last few years, the potential of using derived adjoint-based diagnostic tools has been increasingly exploited.

The influence matrix is a well-known concept in multi-variate linear regression, where it is used to identify influential data and to predict the impact on the initial condition estimates of removing individual data from the regression. The self-sensitivity provides a quantitative measure of the observation influence in the analysis. In the context of 4D-Var there are many components that together determine the influence given to any one particular observation. First there is the specified observation error covariance **R**, which is usually well known and obtained simply from tabulated values. Second, there is the background error covariance **B**, and third, the dynamics and the physics of the forecast model which propagate the covariance in time, and modify it according to local error growth in the prediction. The influence is further modulated by data density.

Forecast sensitivity to observations can be used to diagnose the impact on the short-range forecast, namely 24 to 48 hours, given the use of a simplified adjoint of the data assimilation system and the implied linearity assumption. Forecast error contribution maps allow the geographical identification of beneficial or detrimental observation impact and a clear understanding of the causes can be drawn by the help of observing system experiment (OSE).

The global impact of observations is found to be positive and the forecast errors decrease for all data types. The largest contribution is provided by microwave sounder radiances (AMSU-A) followed by the infrared sounder radiances (IASI and AIRS) from the instruments that mainly provide information on temperature. For satellite humidity information, SSM/I (microwave imager), AMSU-B (microwave sounder), AMSR-E (microwave imager) and MHS (microwave sounder) instruments are the largest contributors to forecast error decrease. In particular, the recent changes applied to the assimilation of all-sky microwave imager radiances increased by a factor of three their mean influence in the analysis (see Geer *et al* 2009; Geer and Bauer 2010) and consequently their impact on the short-range forecast. Since the observation influence decreases with the increase of mean amount of clouds as indicated by model and observations, the most penalized information in the analysis is in a very cloudy regions whilst double DFS is measured on clear-sky ones. Interestingly, in cloudy areas, microwave imager information, is able to decrease the forecast error twice more than in clear sky conditions. It is believed that the largest impact in these areas is mainly due to the larger error present in the forecast in high baroclinic cloudy regions. A similar effect is obtained when the verifying analysis used to compute the forecast error is as the model forecast bias affected. The underestimation of forecast error would therefore directly affect the forecast error reduction computed with the adjoint tool.

Observation System Experiments, used to understand the direct and indirect effect of the assimilation of SSM/I data in specific beneficial areas as indicated by the forecast error contribution maps, highlight that in the Arabian sea during the Monsoon circulation an average reduction of the relative humidity up to 6% on the lower troposphere took place with a consequent reduction of the too strong Monsoon circulation. Instead, over the central Pacific ITCZ, SSM/I have reduced the humidity amount in the upper boundary layer (4%) and increased near surface (2%) causing an intensification of the Hadley circulation that is well known to be too weak in the ECMWF forecast.

Acknowledgements

The authors thank Mohamed Dahoui for the graphical support and Alan Geer to kindly provided the Observation System Experiment. Many thanks also to Peter Bauer for the useful discussion on the observation characteristics and to Jean-Noel Thépaut to improve the manuscript.

References

Baker N.L. and R. Daley, 2000: Observation and background adjoint sensitivity in the adaptive observation targeting problem. *Q. J. R. Meteorol. Soc*, **126**,1431-1454

Bauer, P., A. J. Geer, P. Lopez, and D. Salmond (2010). Direct 4D-Var assimilation of all-sky radiances: Part I. implementation. Quart. J. Roy. Meteorol. Soc., submitted.

Cardinali, C., S. Pezzulli and E. Andersson, 2004: Influence matrix dagnostics of a data assimilation system. *Q. J. R. Meteorol. Soc.*, **130,** 2767—2786

Cardinali, C., and R. Buizza: 2004. Observation sensitivity to the analysis and the forecast: a case study during ATreC targeting campaign. Proceedings of the First THORPEX International Science Symposium, 6-10 December 2004, Montreal, Canada, WMO TD 1237 WWRP/THORPEX N. 6.

Cardinali, C, 2009: Monitoring the forecast impact on the short-range forecast. *Q. J. R. Meteorol. Soc.*, **135,** 239—250.

Chapnik, B., G.Desnrozier, F. Rabier and O. Talagrand, 2004: Property and first application of an error-statistics tuning method in variational assimilation. *Q. J. R. Meteorol. Soc.*, **130,** 2253—2275.

Chapnik, B., G.Desnrozier, F. Rabier and O. Talagrand, 2006: Diagnosis and tuning of observation error in a quasi-operational data assimilation setting. *Q. J. R. Meteorol. Soc.*, **132,** 543—565.

Daescu, D.N., 2008: On the sensitivity equations of four-dimensional variational (4D-Var) data assimilation. *Mon. Wea. Rev.*, **136**, 3050-3065.

Daescu D. and R. Todling 2010: Adjoint sensitivity of the model forecast to data assimilation system error covariance parameters. *Q. J. R. Meteorol. Soc.*, **137,**.

Desroziers G. and Ivanov S. 2001: Diagnisis and adapting tuning of observation error parameters in a variational assimilation. *Q. J. R. Meteorol. Soc.*, **122,** 1433—1452

Errico, R., 2007: Interpretation of an adjoint-derived observational impact measure. *Tellus*, **59A**, 273-276.

Fisher, M., 2003: Estimation of entropy reduction and degrees of freedom for signal for large variational analysis systems. *ECMWF Tech. Memo.*, **397,** pp 18.

Geer, A. J., P. Bauer, and P. Lopez (2010). Direct 4D-Var assimilation of all-sky radiances: Part II. Assessment. Quart. J. Roy. Meteorol. Soc., submitted.

Geer, A.J., and P. Bauer, 2010: Enhanced use of all-sky microwave observations sensitive to water vapour, cloud and precipitation. ECMWF Tec Memo n.620

Gelaro R, Buizza, R., Palmer T.N. and Klinker E., 1998: Sensitivity analysis of forecast errors and the construction of optimal perturbations using singular vectors. *J. Atmos. Sci.*, **55**, 1012—1037.

Hollinger, J., J. Peirce, and G. Poe (1990). SSM/I instrument evaluation. IEEE Trans. Geosci. Remote Sensing 28, 781–790.

Langland R. and N.L Baker., 2004: Estimation of observation impact using the NRL atmospheric variational data assimilation adjoint system. *Tellus,* **56A,** 189-201.

Lorenc, A., 1986: Analysis methods for numerical weather prediction. *Q. J. R. Meteorol. Soc.*, **112,** 1177—1194.

Lopez, P. and E. Moreau, 2005: A convection scheme for data assimilation: Description and initial tests. *Q.J.R.Meteorol.Soc*., **131**, 409—436

Janiskova, M., J.-J. M. J.-F. Mahfouf, and F. Chevallier, 2002: Linearized radiation and cloud schemes in the ECMWF model: Development and evaluation, *Q. J. R. Meteorol. Soc*., **128**, 1505—1527.

Kawanishi, T., T. Sezai, Y. Ito, K. Imaoka, T. Takeshima, Y. Ishido, A. Shibata, M. Miura, H. Inahata and R. Spencer (2003). The Advanced Microwave Scanning Radiometer for the Earth Observing System (AMSR-E), NASDA's contribution to the EOS for global energy and water cycle studies. IEEE Trans. Geosci. Remote Sensing **41**, 184–194.

Morneau J, Pellerin S, Laroche S. and Tanguay M, 2006: Estimation of the adjoint sensitivity gradient in observation space using the dual (PSAS) formulation of the Enviroment Canada operational 4DVar. Proc. Second THORPEX international science symposium, 4-8 Dec 2006, Landshut Germany. WMO TD N.1355 WWRP/THORPEX No.7

Purser, R. J. and Huang, H.-L.,1993: Estimating Effective Data Density in a Satellite Retrieval or an Objective Analysis. *J. Appl. Meteorol.*, **32,** 1092—1107.

Rabier, F., Klinker, E., Courtier, P. and Hollingsworth A. 1996: Sensitivity of forecast errors to initial condition. *Q. J. R. Meteorol. Soc*. **122**, 121—150

Rabier, F., Järvinen, H., Klinker, E., Mahfouf J.F., and Simmons, A., 2000: The ECMWF operational implementation of four-dimensional variational assimilation. Part I: experimental results with simplified physics. *Q. J. R. Meteorol. Soc*. **126,** 1143—1170.

Talagrand, O., 1997: Assimilation of observations, an Introduction. *J. Meteorol. Soc. Japan*, **Vol 75,** N.1B,191—209.

Zhu, Y. and Gelaro, R., 2008: Observation Sensitivity Calculations Using the Adjoint of the Gridpoint Statistical Interpolation (GSI) Analysis System. *Mon. Wea. Rev.*, **136,** 335—351.